Metrol. Meas. Syst., Vol. 28 (2021) No. 2, pp. 371–382
DOI: 10.24425/mms.2021.136613

PAN POLSKA AKADEMIA NAUK

METROLOGY AND MEASUREMENT SYSTEMS

Index 330930, ISSN 0860-8229
www.metrology.wat.edu.pl

M&MS

LAYER THICKNESS MEASUREMENT OF TECHNICALLY ANODISED ALUMINIUM SURFACES BY USING GONIOMETRIC SCATTERED LIGHT

Tobias Geisler, Martin Manns

Universität Siegen, Fakultät IV, Lehrstuhl für Fertigungsautomatisierung und Montage, PROTECH-Institut für Produktionstechnik, Paul-Bonatz-Str. 9-11, 57076 Siegen, Germany (*tobias.geisler@uni-siegen.de*, ✉ *martin.manns@uni-siegen.de*, +49 271 740 5041)

Abstract

In recent years, scattered light measurement technology has developed into a common method for measuring roughness, form and waviness on precision machined surfaces. Meanwhile, the application for the material structure evaluation of electrolytically anodized surfaces has also been considered. In this context, we present a novel approach to layer thickness measurement of naturally anodised aluminium surfaces. Our approach is based on the reflection intensity of the light beam, which penetrates the oxide layer and is reflected back from the surface as well as from the layer base. In the approach, a model for estimating reflection intensity I from the absorption coefficient is employed. The methodology is tested by comparing results to a layer thickness evaluation using metallographic preparation. Based on the proposed approach, we are able to measure intervals of layer thicknesses on naturally anodized aluminium surfaces without contact.

Keywords: anodizing, layer thickness, scattered light, contactless.

1. Introduction

Anodized aluminium materials and components are frequently found in general industry, vehicle construction and building design [12]. For various product properties the measurement of layer thickness plays a central role, since many desired operating and usage properties are a function of layer thickness d_s (Fig. 1), including internal stresses, reflectance, specific electrical resistance and tensile strength. Different technologies employing various physical principles allow measurement of layer thickness in the range of 3 nm up to 50 μm.

In most thickness measurement technologies, a sensor must be placed on the surface. Although this is considered non-destructive measurement, time requirements are an issue for practical applications such as mass production of extruded or rolled products [23].

Therefore, contact free measurements of larger segments would be beneficial for efficiency of in line measurements in production lines.

Article history: received July 6, 2020; revised January 11, 2021; accepted January 19, 2021; available online March 19, 2021.

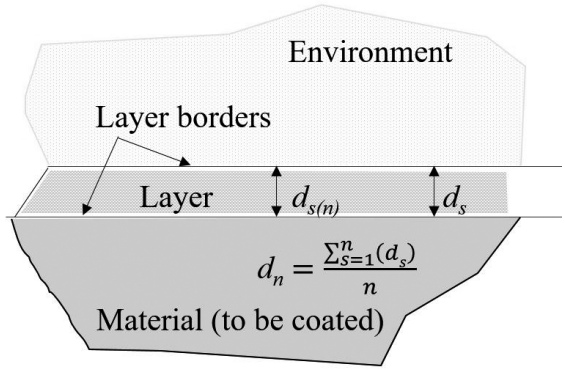

Fig. 1. Layer thickness d_s.

Eddy current sensors are able to measure the layer thickness of electrical insulators on opaque objects. They penetrate the insulating layer without interference and measure the distance to the layer behind it. At the same time, a second sensor, $e.g.$ a laser triangulator, a capacitive sensor or an optical micrometer measures the insulating layer. The thickness of the layer is determined by calculating both signals.

Another commonly employed measurement technology is measuring layer thickness of transparent materials with confocal measurement. Here, the light penetrates the measured object and provides a peak in the signal graph at each transition as for example with a Perspex panel.

In contrast to the measuring methods described above, scattered light approaches are able to detect microstructural surface properties such as roughness without contact and with higher speed on larger surfaces [2, 4]. The technology is already used for dielectric and therefore practically non-absorbent layers and enables the production of mirrors with high reflection values [20]. In the case of unpolished samples with diffuse reflection there are first approaches to use scattered light for evaluation processes [9]. The scattered light approach to the measurement of thin-film samples with a commercial ellipsometer is described in [25]. In these tests, scattered light technology provides higher accuracy than thin-film measurements, which may make scattered light technology promising for probing arbitrary heterogeneities in surfaces and fills [6]. However, nowadays scattered light technology is not commonly used for thickness measurements of thick, crystalline and porous layers in failure-prone production environments.

In this paper we present a new approach to measuring the thickness of anodized aluminium surfaces using scattered light. We propose

- a methodology for detecting surface thickness over large sections using our scattered light approach, and
- a fast classification methodology for the measurement of oxide layers according to results of thickness evaluation via metallographic preparation.

The main sections of this paper are presented as follows. In Section 2, we review previous research on thickness measurements by optical and electromagnetic technologies and give an introduction of scattered light opportunities. In Section 3, we give an overview over our approach to evaluating anodized layers, which implements a comparison measurement to thickness evaluation via subsequent microstructure preparation and microscopy. Identification capabilities of layer thicknesses and their objective derivation are shown in Section 4. We conclude the paper with a discussion about the results of our research.

2. State of the art

2.1. Layer thickness

Layer thickness d_s is specified as the distance between the intersection points of the two layer borders:

- *True layer thickness* d_s: (Fig. 1) according to the definition given above, but usually only on local very limited areas (local size).
- *Average layer thickness* d_n: Thickness specification which is derived from a physical measured quantity, e.g. surface resistance is determined. The thickness and the measured value are displayed in a known, reproducible relationship that can be described by a function. Average layer thickness represents an average value over the true layer thicknesses.

2.2. Non-destructive measuring methods

There are numerous methods for determining the thickness of oxide layers. During production, however, these layers should not be damaged as a result of surface evaluation.

The *Eddy Current Measuring Method* is an electromagnetic coating thickness measuring method. The process is suitable for non-destructive measuring of both electrically non-conductive coatings (like ceramic or anodised) on non-ferromagnetic but electrically conductive base materials and electrically conductive coating materials on insulating or poorly conducting substrates. A high-frequency current flowing in a coil placed close to the base material generates a changing magnetic field. The field produces eddy currents in the base material that can be monitored using either another coil or by measuring changes of the current in the primary coil. The magnetic field of the coil decreases with increasing distance from the surface of the base coating. According to Lenz's rule [7], it is overlaid by the eddy currents-generated magnetic field and becomes weaker. Thus the impedance of the coil changes, depending on the distance of the probe from the base material, as a measured variable for the coating thickness [5].

Based on the *Electromagnetic Flux Leakage* (EMFL), wall thicknesses of various materials such as gas pipes, are measured. This is done by means of equivalent magnetic circuit analysis and finite element analysis [25].

Ultrasonic process sensors are also suitable for detection of gaseous, liquid or molten layers. Besides temperature and pressure, other process parameters such as level, flow and turnover are of particular interest. Main applications are found in the food, chemical and pharmaceutical industries. In solid materials, ultrasonic sensors are used to find pores or inclusions, and this technique is also suitable for measuring distances. In the detection of rigid and crystalline layers the technology reaches its limits [11].

The *Roentgen Radiation Fluorescence* (XRF) is a phenomenon which can be used for the measurement of coating thickness and material analysis. It can be used for the qualitative and quantitative determination of elementary composition of a material sample and for measuring coatings and coating systems. The principle behind the XRF is that electrons are released from inner shells of atoms in a material sample when it is bombarded with X-rays or gamma rays. As this makes the atoms energetically unstable, the resulting gaps are filled up by electrons from atomic shells located further out which, in turn, causes emission of secondary X-rays i.e. fluorescent radiation, characteristic for each element. When detected, it can provide information about the composition of the sample [19]. At the same time, the intensity of X-ray fluorescence radiation of the coating components can be used as a measure of the coating thickness and can

be determined by comparison with known coating thicknesses of the same material composition calibrated under identical test conditions.

2.3. Destructive measuring method

A precise but destructive method for measuring coating thicknesses is *metallographic examination* – with subsequent microstructure preparation and microscopy. For this approach, the workpiece must be cut out and then ground and polished with a grinding machine and polishing machine. The coating thicknesses are analyzed under an optical microscope at a magnification of 50 to 1,000 times (typical and sufficient: 500× magnification) [14]. The effort is accordingly high and the workpiece is destroyed.

2.4. Light properties

The term "optical" or "thin" coating refers to layers whose physical thickness is in the range of the light wavelength, *i.e.* for visible light on the order of a few hundred nanometres [13]. At such layers, electromagnetic radiation of the corresponding wavelength can interfere. However, this requires a change in the refractive index at the interfaces of the layer so that part of the light is reflected. In addition to reflection, translucent materials allow a certain proportion of rays to pass through (transmission) and stop part of them by absorption. The sum of the reflections, transmission and absorption and the residual ray is always 100 percent of the incident light beam.

The decrease in transmission in clear and liquid layers is not proportional to the increase in thickness of the entire layer.

This effect can be described with the Beer–Lambert law, see [13, 22]. The calculation can only be performed if the layer is irradiated with monochromatic light or if K is known for the used wavelengths λ_0, shown in (1). The light absorption during transmission depends on the *absorption coefficient* α, which is based on the *extinction coefficient* of the irradiated material. For sufficiently diluted solutions and purely crystalline substances, α is proportional to v of the absorbing particles dissolved, formulated as

$$\alpha = \frac{4 \cdot \pi \cdot K}{\lambda_0}, \tag{1}$$

included in

$$T(d, \alpha) = e^{-\alpha \cdot d}. \tag{2}$$

2.5. Light scattering

An essential method for measuring light is the *angle-resolved light scattered measurement* (ARS). ARS records reflectance intensities for discrete profile angles φ_i, $i = 1, \ldots, n$, backscattered by a small surface region (spot) with diameter d, which in turn is illuminated by a laser. The profile angles φ_i are gathered by a photosensitive linear detector comprising a number of n photodiodes. The angle of the incident light depends on the illuminated area of the LED. Therefore a correction of the surface gradient is performed to ensure the parallelism of the incident light. It can also be assumed that the density of the illumination is almost uniform. The reflected light is collected by the measuring lens and projected onto an intensity detector, a small array of diodes aligned in the x-direction of the surface topography [21]. The detector array detects the irradiated spot and, at the time of measurement, gives an intensity curve which represents power to area and

is calculated back to the reflecting surface. Figure 2 depicts this setup which measures the *single reflection intensity* $I(\varphi_i')$ [21] for angle φ_i captured at a *normalized position* φ_i' on the detector array, where $\varphi' = \tan(\varphi)$. From this, *standardized distribution of scattering angles* $H(\varphi)$ and *focus of distribution curve M* are derived [16]:

$$I = \sum_{i=1}^{n} I\left(\varphi_i'\right), \qquad H\left(\varphi_i\right) = \frac{I\left(\varphi_i'\right)}{I}. \tag{3}$$

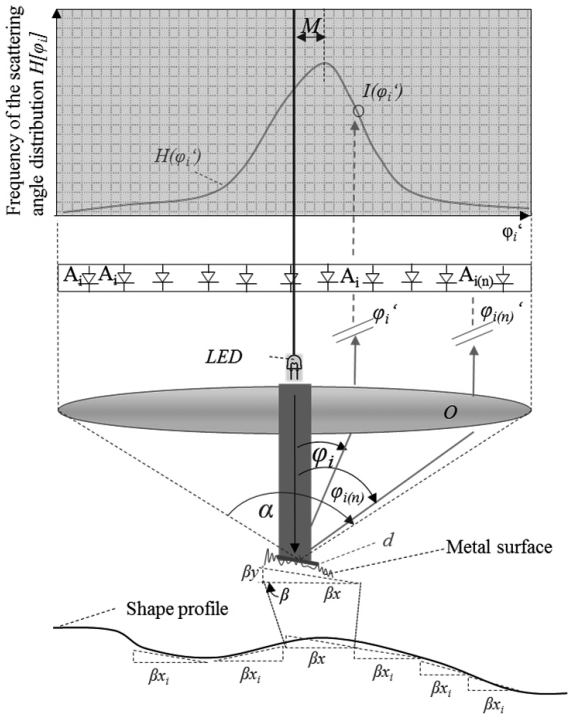

Fig. 2. The ARS measuring principle [3].

This non-destructive measuring methods is capable of covering larger surface areas, which makes it applicable for a quick online quality control For example a classification of stripes or inhomogeneous structures can be evaluated [8] with this method. For layer thickness of anodized surfaces, we derive quality parameters that relate to the reflection intensities obtained from the scattered light.

ARS analyzes the surface properties of materials, but it is not yet or rarely used for material layer and depth dimension analysis of a translucent layers. We present a practice-oriented method for this purpose, which is based on an analytical model.

3. Evaluation setup of layer thickness measurement via ARS

Derived from the Beer–Lambert law (see (2)), we present our "Light Model" of a technically produced oxide layer; see Fig. 3. The test setup selected in Subsection 3.2 was chosen to verify our developed model.

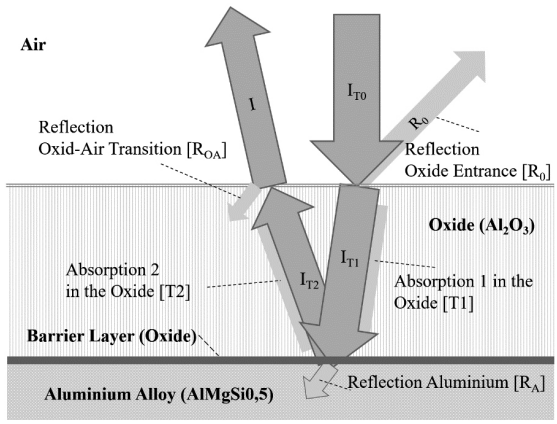

Fig. 3. Light Loss of Aluminium Oxide.

3.1. Light model of anodized aluminium

As described in Subsection 2.4, light can be absorbed or reflected when passing from air to another material. In our data model, this energy can be divided into partial absorptions of several materials. Figure 7 shows the structure of a typical technical oxide coating on aluminium. This consists essentially of an oxide top layer consisting of pores and crystals, a barrier layer in structure similar to a thin film and the base aluminium itself; see Fig. 3. Multiple reflections through the pores were deliberately not considered. Instead in order to derive a simple, practically applicable model, they are included in the absorption values of the double light transmissions, based on incoming light and the light reflected at the boundary layer.

Each material has its own transmission behavior, which is influenced by specific absorption and reflection values, as described in Subsection 2.4. The respective energy absorption or reflection of one material must therefore be considered as a subtraction in the output energy for the behavior of the next material. The following Table 1 shows the specific characteristics for the respective material components for the absorption coefficient and reflection index.

Table 1. Model Parameters [3, 10, 13, 15, 18].

Parameter Description	Index	Physical Entity	Value of Unit
Light Figures (Scattered Light Units are relative Units, see Subsection 2.5)			
Light Source Intensity	I_{T0}	mW/m^2	3480
Laser Wave Length	λ	µm	0.679
Transmission Figures			
Reflection Air – Oxide Entrance	R_0	%	7.4
Reflection Aluminium – Air	R_{0A}	%	0.1
Reflection Aluminium	R_A	%	10.9
Absorption Coefficient Oxide Al_2O_3 (Thin Film / Crystal)	α	µm^{-1}	0.29 / 0.37
Extinction Coefficient Oxide Al_2O_3 (Thin Film / Crystal)	k		0.016 / 0.019

I_m is calculated following (4) to (6):

$$I_{T1} = (1 - R_0) I_{T0}\,, \tag{4}$$

Metrol. Meas. Syst., Vol. 28 (2021), No. 2, pp. 371–382
DOI: 10.24425/mms.2021.136613

$$I_{T2} = (1 - R_A)\, \mathrm{e}^{-a \cdot d} I_{T1}\,, \tag{5}$$

$$\boldsymbol{I}_m = (\mathbf{1} - \boldsymbol{R}_{0A})\, \boldsymbol{e}^{-a \cdot d} \boldsymbol{I}_{T2} + \boldsymbol{R}_0 \boldsymbol{I}_{T0}\,. \tag{6}$$

3.2. Setup of the measurement

In order to achieve the most accurate measurement, metallographic analysis was chosen as the evaluation measurement result because of the round sample and hollow chambers geometry. Alternatively, the samples measured with scattered light were evaluated by metallographic preparation, see Fig. 5. For this purpose, 50 specimens of various coating thickness were carried out on a 20 mm measuring length. The basis of the sample pieces was an extruded aluminium profile which was subsequently anodized. For the measurement, 100 mm pieces were cut out. An OS 500 scattered light sensor [3] was used in conjunction with a UR5e Universal Robot for evaluation. For this purpose, the exact measuring range was predefined and scanned. The 3D shape geometries of the samples were previously read into the sensor database of the robot and the measuring range was defined in the model of the shape section. In this way, the robot software provided the geometry and position of the points to be measured and followed the measuring paths automatically. The robot was programmed with the help of working points. The individual test points were read via a teach-in procedure. At the same time, the simulation of the robot's movement was used to optimize error detection on the robot program created offline. In the control software, a "batch" was created for each sample, in which all specific data of the measurement are entered. Multiple measurements were always carried out over a length of X mm and a number of individual measurements I. The quotient of the length X and the number I gave the resolution Delta X mm. The highest possible resolution, *i.e.* a measuring distance of 0.125 mm, was selected for the test series. The measuring point had a diameter of 0.03 mm. The following schematic block diagram (Fig. 4) shows the process in detail.

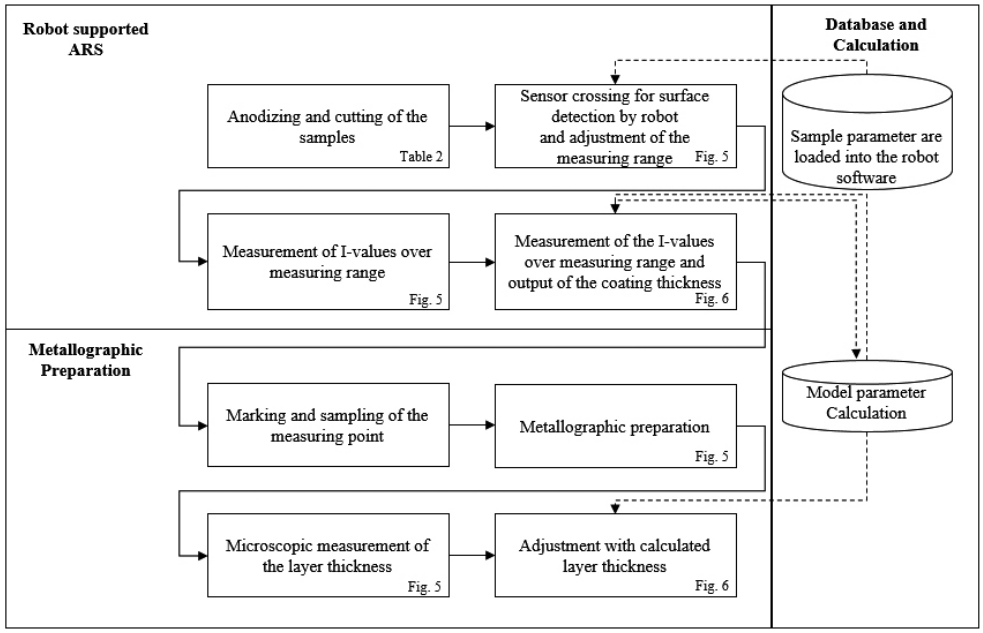

Fig. 4. Schematic Block Diagram of the Measurement.

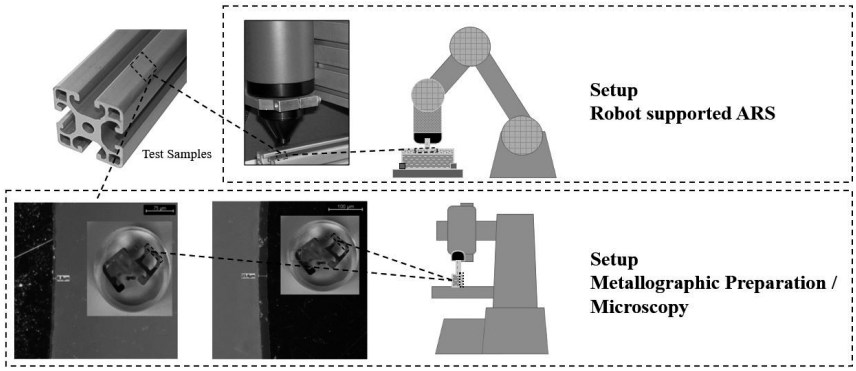

Fig. 5. Test Setups ARS and Microscopy.

As shown in the Block Diagram (Fig. 4), subsequently the same measuring points were prepared by grinding, polishing and chemical etching. In a second step the coating thickness was evaluated with microscopic length measurement using an *Axiocam 305 color* digital camera in combination with a *Carl Zeiss JENAPHOT2000.*

In order to carry out the desired comparative measurements, 4 main samples were prepared in the form of extrusions. From these the 50 individual specimens were taken. Special care was taken to ensure that normal material structure was produced. The essential decision criterion is the grain size. This was set to 4 ASTM [1] in order to standardize the influence of different grain boundary reflections in ARS. The subsequent anodizing of the base material was then adjusted according to the process described in Table 2.

Table 2. Setting of the Coating Thickness.

Process Step	**Duration [min]**	**Parameter**	**Physical Entity**	**Medium**
Degreasing	20	60	°C	50 g/l Degreasers
Rinsing	1	20	°C	H_2O
E6-Etching	10	69	°C	55 g/l NaOH 105g/l Al 33 g/l Etching Additive
Rinsing	1	20	°C	H_2O
Special Etching – Decapering	1	20	°C	120 g/l HNO_3
Rinsing	1	20	°C	H_2O
Anodizing / GS process		20	°C	
Setting Coating Thickness	5	5	µm	190 g/l H_2SO_4 4 g/l Al
	14	10	µm	
	20	15	µm	
	26	20	µm	
Rinsing	2	20	°C	H_2O
Spray Rinsing	1	20	°C	VE-H_2O
Hot Sealing	3 (min/µm)	96	°C	VE-H_2O 1.5 ml/l Preventing deposits

Metrol. Meas. Syst., Vol. 28 (2021), No. 2, pp. 371–382
DOI: 10.24425/mms.2021.136613

4. Results

Using the test setup described in Section 3, 202 evaluable measurements were conducted. Fig. 6 displays both the analytically predicted and the measured light intensity I_m for different Al_2O_3 layer thicknesses. The top left diagram visualizes the analytical functional relation as a curve and the measurement results as a scatter plot. The bottom left diagram displays the differences between the measurements and the curve, which clarifies systematic deviations. The bottom right histogram depicts the quantitative distribution of deviations. For thicknesses below 7 µm, the analytical model clearly overestimates I_m.

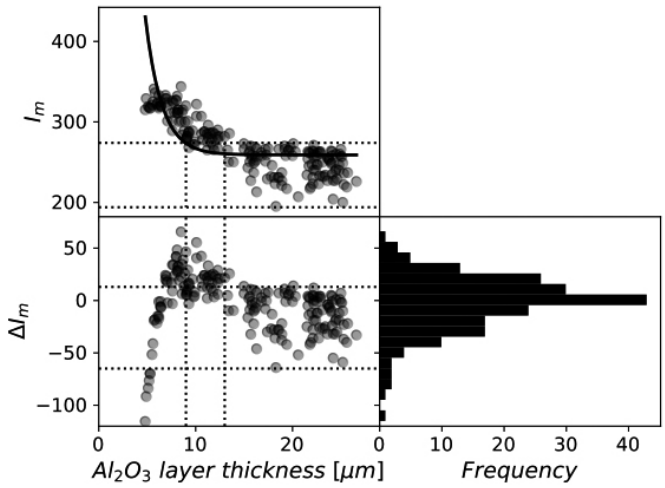

Fig. 6. Measured vs. analytically predicted light intensity; Thin Film. ΔI_m refers to the difference between analytically estimated and measured light intensity.

For thicknesses between 9 and 13 µm, it underestimates I_m. For thicknesses above 13 µm, the analytical results seems to be situated below an upper limit for I_m, while for some measurements, the analytical model again overestimates I_m. Overall, considerable deviations are observable.

The analytical model converges at an $I_m = 259$. There is an upper bound of measured values, not increasing for large Al_2O_3 layer thicknesses which confirms this prediction qualitatively. The analytically predicted value matches the upper limit of the measured reflections reasonably well. The cause for the decreased light intensity for some specimen at thicknesses above 13 µm is unclear. It is assumed that the effect of multiple reflection and transmission becomes more and more pronounced due to the ever larger pores. In addition, it is to be said that the thickness of the pore wall decreases more and more due to its own growth. This can lead to the fact that the light rays penetrate them, are weakened by the transmission and are reflected in the next pore. This, in turn, leads to cross scattering which can no longer be detected by the diode array due to its limited angle α, see Fig. 2.

5. Discussion

The analytically predicted decline in intensity of the scattered light can principally be observed with the proposed methodology. However, there is considerable residual error which is partly systematic. In order to explain this residual defect in terms of materials, we consider the

microscopic structure of an oxide layer; see Fig. 7. On the right side you can see a *Scanning Electron Microscope* (SEM) image of an anodized layer. Pores are formed due to the chemical growth of the layer [17, 24]. When light enters a pore, multiple reflections occur along the pore wall. If the light hits the pore edge, it is additionally partly absorbed. According to *Beer–Lambert*, the influence of the absorption effect decreases with increasing layer thickness until almost no more light is transmitted. The combination of both effects can lead to the described error.

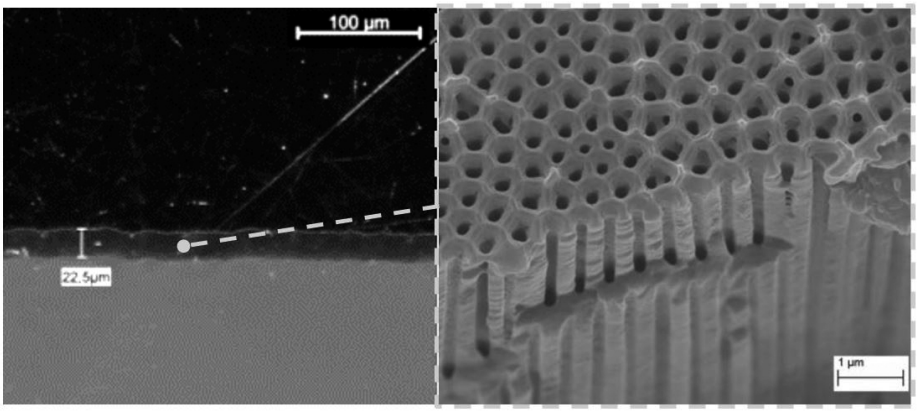

Fig. 7. Microstructure of an Anodized Layer (Al_2O_3) [15].

Considering the measured error, the test shows that our methodology can be applied to determine if a layer is thicker than 9 µm or not. The systematic error below 7 µm imposes an upper limit to the measured light intensity and therefore does not affect the aforementioned application.

There seems to be an offset of 1 µm in layer thickness between the analytical and the measured result. The pore channels with a diameter of about 0.01 to 0.05 µm expand to surface. If a pore forms up to the metal during oxidation, the electrolyte moves into the pore. Since there are many pores next to each other, the oxide layer grows evenly into the metal. This layer grows proportionally to the overall view, but is only a few nm to µm thick in proportion. Since the layer is a pore-free one, it has a more reflective effect like a thin film instead of absorbing and this could explain the uniform offset of 1 µm.

If the offset could be explained and residual error compensated, the measurement could be improved so that two or more intervals of layer thickness may be determined.

6. Conclusions

In this paper we present a new approach to assessment of oxide layer thicknesses of anodized aluminium using scattered light. For this purpose a simple analytical model was developed, which was verified by comparing the light energy, measured by scattered light technique, with the thickness measurement by metallographic preparation. We successfully apply our method for a first interval detection of oxide layer thicknesses on anodized aluminium profiles. This allows the thickness of the layer to be determined during series production without having to touch the surface or take samples. Thus, the process parameters can be adjusted online to prevent possible errors during anodizing from the beginning. During the measurement a residual error occurred,

which turned out to be limited to a layer thickness of less than 9 µm. Therefore, it is already possible to perform a determination from 9 µm in a first interval. If the occurrence of the error can be deduced, it will be possible to carry out further improvement steps.

References

[1] ASTM International. (2015). Standard Test Methods for Determining Average Grain Size (ASTM E112 – 13). https://doi.org/10.1520/E0112-13

[2] Brodmann, R., & Allgauer, M. (1989). Comparison of light scattering from rough surfaces with optical and mechanical profilometry. *Proceedings of the International Congress on Optical Science and Engineering, France*, *1009*, 111–118. https://doi.org/10.1117/12.949161

[3] OptoSurf Gmbh. (2014). Datas Sheet OS 500-32.

[4] Brodmann, R., & Thurn, G. (1986). Roughness measurement of ground, turned and shot-peened surfaces by the light scattering method. *Wear*, *109*(1–4), 1–13. https://doi.org/10.1016/0043-1648(86)90247-4

[5] Cheng, W. (2017). Thickness measurement of metal plates using swept-frequency eddy current testing and impedance normalization. *IEEE Sensors Journal*, *17*(14), 4558–4569. https://doi.org/10.1109/JSEN.2017.2710356

[6] Choi, G., Kim, M., Kim, J., & Pahk, H. J. (2020). Angle-resolved spectral reflectometry with a digital light processing projector. *Optics Express*, *28*(18), 26908–26921. https://doi.org/10.1364/OE.405204

[7] Duffy, A. (2018). A pictorial approach to Lenz's law. *The Physics Teacher*, *56*(4), 224–225. https://doi.org/10.1119/1.5028236

[8] Geisler, T., & Kolb, A. (2018). Pattern recognition of rough surfaces by using goniometric scattered light. *Metrology and Measurement Systems*, *25*(1), 33–46. https://doi.org/10.24425/118160

[9] Gilbert, O., Deumié, C., & Amra, C. (2005). Angle-resolved ellipsometry of scattering patterns from arbitrary surfaces and bulks. *Optics Express*, *13*(6), 2403–2418. https://doi.org/10.1364/OPEX.13.002403

[10] Hagemann, H. J., Gudat, W., & Kunz, C. (1975). Optical constants from the far infrared to the x-ray region: Mg, Al, Cu, Ag, Au, Bi, C, and Al 2 O 3. *Journal of the Optical Society of America*, *65*(5), 742–44. https://doi.org/10.1364/JOSA.65.000742

[11] Hauptmann, P., Hoppe, N., & Püttmer, A. (2002). Application of ultrasonic sensors in the process industry. *Measurement Science and Technology*, *13*(8), 73–83. https://doi.org/10.1088/0957-0233/13/8/201

[12] Lane, J. (1992). *Aluminium in Building*. Routledge. https://doi.org/10.4324/9780429463372

[13] Aslan, M. M., Webster, N. A., Byard, C. L., Pereira, M. B., Hayes, C. M., Wiederkehr, R. S., & Mendes, S. B. (2010). Low-loss optical waveguides for the near ultra-violet and visible spectral regions with Al_2O_3 thin films from atomic layer deposition. *Thin Solid Films*, 518(17), 4935–4940. https://doi.org/10.1016/j.tsf.2010.03.011

[14] Nicholson, R. B., Thomas, G., & Nutting, J. (1958). A technique for obtaining thin foils of aluminium and aluminium alloys for transmission electron metallography. *British Journal of Applied Physics*, *9*(1), 25. https://doi.org/10.1088/0508-3443/9/1/305

[15] Nielsch, K., Choi, J., Schwirn, K., Wehrspohn, R. B., & Gösele, U. (2002). Self-ordering regimes of porous alumina: the 10 porosity rule. *Nano letters*, *2*(6), 677–680. https://doi.org/10.1021/nl025537k

[16] Deutscher Verband der Automobilindustrie. (2009). Geometrische Produktspezifikation Oberflächenbeschaffenheit Winkelaufgelöste Streulichtmesstechnik Definition, Kenngrößen und Anwendung (Norm VDA 2009 2010-07-00).

[17] Parkhutik, V. P., & Shershulsky, V. I. (1992). Theoretical modelling of porous oxide growth on aluminium. *Journal of Physics D: Applied Physics*, *25*(8), 1258. https://doi.org/10.1088/0022-3727/25/8/017

[18] Querry, M. R. (1985). *Optical constants*. University of Missouri – Kansas City.

[19] Revenko, G. (2000). X-RAY Fluorescence Analysis: State of the Art and Trends of Development. Industrial Laboratory. Diagnostics of Materials, *66*(10), 637–652.

[20] Schröder, S., Herffurth, T., Blaschke, H., & Duparré, A. (2011). Angle-resolved scattering: an effective method for characterizing thin-film coatings. *Applied Optics*, *50*(9), C164–C171. https://doi.org/10.1364/AO.50.00C164

[21] Seewig, J., Beichert, G., Brodmann, R., Bodschwinna, H., & Wendel, M. (2009). Extraction of shape and roughness using scattering light. *SPIE Europe Optical Metrology, Optical Measurement Systems for Industrial Inspection VI*, *7389*, 73890N. https://doi.org/10.1117/12.827478

[22] Swanepoel, R. (1983). Determination of the thickness and optical constants of amorphous silicon. *Journal of Physics E: Scientific Instruments*, *16*(12), 1214–1218. https://doi.org/10.1088/0022-3735/16/12/023

[23] Sweeney, K., & Grunewald, U. (2003). The application of roll forming for automotive structural parts. *Journal of Materials Processing Technology*, *132*(1–3), 9–15.

[24] Wolter H. (1956) Optik dünner Schichten. In Bergstrand, E., Maréchal, A., Françon, M., & Wolter, H. (Eds.) *Grundlagen der Optik/Fundamentals of Optics* (pp. 461–554), Springer Verlag. https://doi.org/10.1007/978-3-642-45850-7_4

[25] Zhang, Y., & Yan, G. (2007). Detection of gas pipe wall thickness based on electromagnetic flux leakage. *Russian Journal of Nondestructive Testing*, *43*(2), 123–132. https://doi.org/10.1134/S1061830907020088

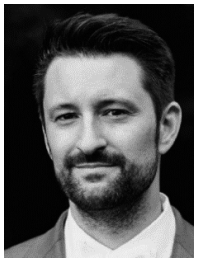

Tobias Geisler (M.Eng.) completed his education in metallography and material technology in Solingen, Germany, studied mechanical engineering and received his Master degree in production technologies in 2012. Currently he is preparing his PhD thesis at the Institute for Manufacturing Automation and Assembly (FAMS) at the Universität Siegen. During his industrial career, he developed special machines and was Head of Technical Procurement at item Industrietechnik GmbH. He is CEO of TriniDat Software-Entwicklung GmbH.

Martin Manns (Prof. Dr.-Ing.) is holding the Chair for Manufacturing Automation and Assembly (FAMS) at the Universität Siegen. After receiving a doctorate in mechanical engineering, he continued research at the University of Windsor, ON, Canada. His industrial experience comprises positions at SIG Positec Berger Lahr GmbH, Henkel AG & Co KGaA and Daimler AG. His research interest comprises smart manufacturing, assembly planning, human motion modeling and soft and collaborative robotics.